University Library

MINERVA ACCESS

A gateway to Melbourne's research publications

Minerva Access is the Institutional Repository of The University of Melbourne

Author/s:
Niu, S;Jiang, WJ;Tang, T;Yuan, LP;Luo, H;Hu, JS

Title:
Autogenous Growth of Hierarchical NiFe(OH)x/FeS Nanosheet-On-Microsheet Arrays for Synergistically Enhanced High-Output Water Oxidation

Date:
2019-09-01

Citation:
Niu, S., Jiang, W. J., Tang, T., Yuan, L. P., Luo, H. & Hu, J. S. (2019). Autogenous Growth of Hierarchical NiFe(OH)x/FeS Nanosheet-On-Microsheet Arrays for Synergistically Enhanced High-Output Water Oxidation. Advanced Functional Materials, 29 (36), https://doi.org/10.1002/adfm.201902180.

Persistent Link:
https://hdl.handle.net/11343/286097

Check for updates

Autogenous Growth of Hierarchical $NiFe(OH)_x$/FeS Nanosheet-on-Microsheet Arrays for Synergistically Enhanced High-Output Water Oxidation

*Shuai Niu, Wen-Jie Jiang, Tang Tang, Lu-Pan Yuan, Hao Luo, and Jin-Song Hu**

S. Niu, Dr. W.-J. Jiang, T. Tang, L.-P. Yuan, Dr. H. Luo, Prof. J.-S. Hu

Beijing National Laboratory for Molecular Sciences (BNLMS),

CAS Key Laboratory of Molecular Nanostructure and Nanotechnology,

Institute of Chemistry, Chinese Academy of Sciences (CAS),

Beijing 100190, China

E-mail: hujs@iccas.ac.cn

S. Niu, Dr. W.-J. Jiang, T. Tang, L.-P. Yuan, Prof. J.-S. Hu

University of Chinese Academy of Sciences

Beijing 100049, China

Keywords: hierarchical structures, sheet-on-sheet, FeS, oxygen evolution reaction, water splitting

Author Manuscript

This is the author manuscript accepted for publication and has undergone full peer review but has not been through the copyediting, typesetting, pagination and proofreading process, which may lead to differences between this version and the Version of Record. Please cite this article as doi: 10.1002/adfm.201902180.

This article is protected by copyright. All rights reserved.

Abstract

Practical electrochemical water splitting requires cost-effective electrodes capable of steadily working at high output with a small overpotential, leading to the challenges for efficient and stable electrodes for oxygen evolution reaction (OER). Herein, by simply using conductive FeS microsheet arrays vertically pre-grown on iron foam (FeS/IF) as both substrate and source to in-situ form vertically aligned $NiFe(OH)_x$ nanosheets arrays, a hierarchical electrode with a nano/micro sheet-on-sheet structure ($NiFe(OH)_x$/FeS/IF) can be readily achieved to meet the requirements. FeS/IF not only acts as a 3D microporous conductive scaffold to enable efficient electron/mass transfer but also provides high surface area for integrating more highly active $NiFe(OH)_x$ sites. Such hierarchical electrode architecture with superhydrophilic surface also allows for prompt gas release even at high output. As a result, $NiFe(OH)_x$/FeS/IF exhibits a superior OER activity with an overpotential of 245 mV at 50 mA cm^{-2} and can steadily output 1000 mA cm^{-2} at a low overpotential of 332 mV without appreciable interference by intensive gas evolution. The water-alkali electrolyzer using $NiFe(OH)_x$/FeS/IF as anode can deliver 10 mA cm^{-2} at 1.50 V and steadily operate at 300 mA cm^{-2} with a small cell voltage for 70 hours. Furthermore, a solar-driven electrolyzer using the developed electrode demonstrates an exceptional high solar-to-hydrogen efficiency of 18.6%. Such performance together with low-cost Fe-based materials and facile processing compatible with cost-effective mass production suggest that the present strategy may open up opportunities for rationally designing hierarchical electrocatalysts for practical water splitting or diverse applications.

Author Manuscript

This article is protected by copyright. All rights reserved.

Electrochemical water splitting is regarded as a promising technique to produce clean and sustainable energy (hydrogen), while the kinetics of oxygen evolution reaction (OER) at anode is still sluggish thus limits the efficiency of water splitting owing to the complex four-step proton-coupled electron transfer processes.[1] From the viewpoint of practical application, the anode electrode needs to meet the following requirements at least: 1) high activity for OER to reduce electricity consumption, not only at a small current density but also at a practical current density up to hundreds of mA cm^{-2}; 2) stable and high output for meaningful hydrogen production at industrial scale, involving in large current density and continuously intensive gas evolution; 3) low cost for both electrode materials and scalable production process. Although the research progress have been recently made in a couple of years,[2] it is still necessary but challenging to develop effective OER electrodes meeting these industrial requirements.

A durable efficient OER electrode firstly needs sufficient chemically stable catalytic sites with high intrinsic activity. Metal hydroxides are good candidates in view of their chemical stability in operational conditions and high OER activity. Among them, NiFe bimetallic hydroxide ($NiFe(OH)_x$) exhibits the best intrinsic OER activity in alkaline solution due to the strong synergistic effect between the metal centers, although the genuine catalytic sites and underlying mechanisms are not fully understood yet.[3] Nevertheless, the Achilles heel of $NiFe(OH)_x$ is poor conductivity, limiting its catalytic activity especially at large current density. Coupling $NiFe(OH)_x$ with conductive substrates such as carbon nanotube, graphene, copper or nickel foam has been proved as an effective way to alleviate this issue.[4] However, there is still much room for further improving its OER performance at high output by rationally designing electrode architectures and the synthetic methods need to be simplified in terms of mass production.

Author Manuscript

This article is protected by copyright. All rights reserved.

Secondly, the stable and high-output oxygen generation requires the electrode to be able to deal with highly intensive electron transportation and mass transfer, prompt and efficient gas release, as well as high duty with mechanical stability. Highly conductive three-dimensional (3D) robust substrates such as metal foam with massive macropores would be good options, although the delicate structural design upon incorporating catalytic materials should be considered since the large surface area is necessary for exposing catalytic sites as much as possible.[5] The swift gas release to avoid the blocking of catalytic centers during OER commonly demands 3D textured electrode surface with a high roughness factor and hydrophilic nature. The vertically aligned one-dimensional (1D) nanowire arrays has been demonstrated to be highly effective for gas escaping. Considering the mechanical durability, two-dimensional (2D) nanosheet arrays holding both much larger contact at microscale with substrate and small thickness at nanoscale for exposing more catalytic sites as well as high roughness factor might be more suitable. Lastly, from the views of practical hydrogen production, the cost-effective materials and mass production with facile and scalable processing are also necessary for designing an OER electrodes.

To fulfill these requirements simultaneously, we rationally design herein a facile and scalable strategy for fabricating a hierarchically structured OER electrode with vertical $NiFe(OH)_x$ nanosheets on iron sulfide (FeS) microsheet arrays vertically grown on 3D microporous iron foam (IF). Such hierarchical electrode (denoted as $NiFe(OH)_x$/FeS/IF) holds the following features: 1) The highly conductive mackinawite FeS microsheet arrays on Fe foam not only acts as a 3D conductive scaffold with massive macropores for efficient electron transportation and mass transfer, but also provides high surface area for loading more $NiFe(OH)_x$; 2) $NiFe(OH)_x$ nanosheet arrays vertically grown on FeS microsheet arrays enable a sufficient amount of chemically stable and accessible catalytic sites to catalyze OER; 3) 3D hierarchical nano/micro sheet-on-sheet array architecture allows for prompt gas

Author Manuscript

This article is protected by copyright. All rights reserved.

release; 4) The strategy using Fe foam as both substrate and Fe source to grow FeS microsheet scaffold which is subsequently used to grow $NiFe(OH)_x$ makes the electrode mechanically stable during intensive gas evolution; 5) The low-cost starting material of iron, one of the most earth-abundant element,[6] and the simple preparing procedures make the electrode and processing cost-effective and scalable for mass production. As a result, $NiFe(OH)_x$/FeS/IF exhibits superior OER activity with small overpotentials of 245 and 261 mV to reach 50 and 100 mA cm^{-2}, respectively, which are much lower than the values for most reported bimetallic hydroxides composites. Notably, high current densities of 500 and 1000 mA cm^{-2} could be steadily output at low overpotentials of 304 and 332 mV, respectively. A water-alkali electrolyzer is further demonstrated to stably and continuously output a high current density of 300 mA cm^{-2} at 1.95 V for over 70 h. These results may shed lights on exploring practical OER electrodes for industrial electrochemical water splitting.

Author Manuscript

This article is protected by copyright. All rights reserved.

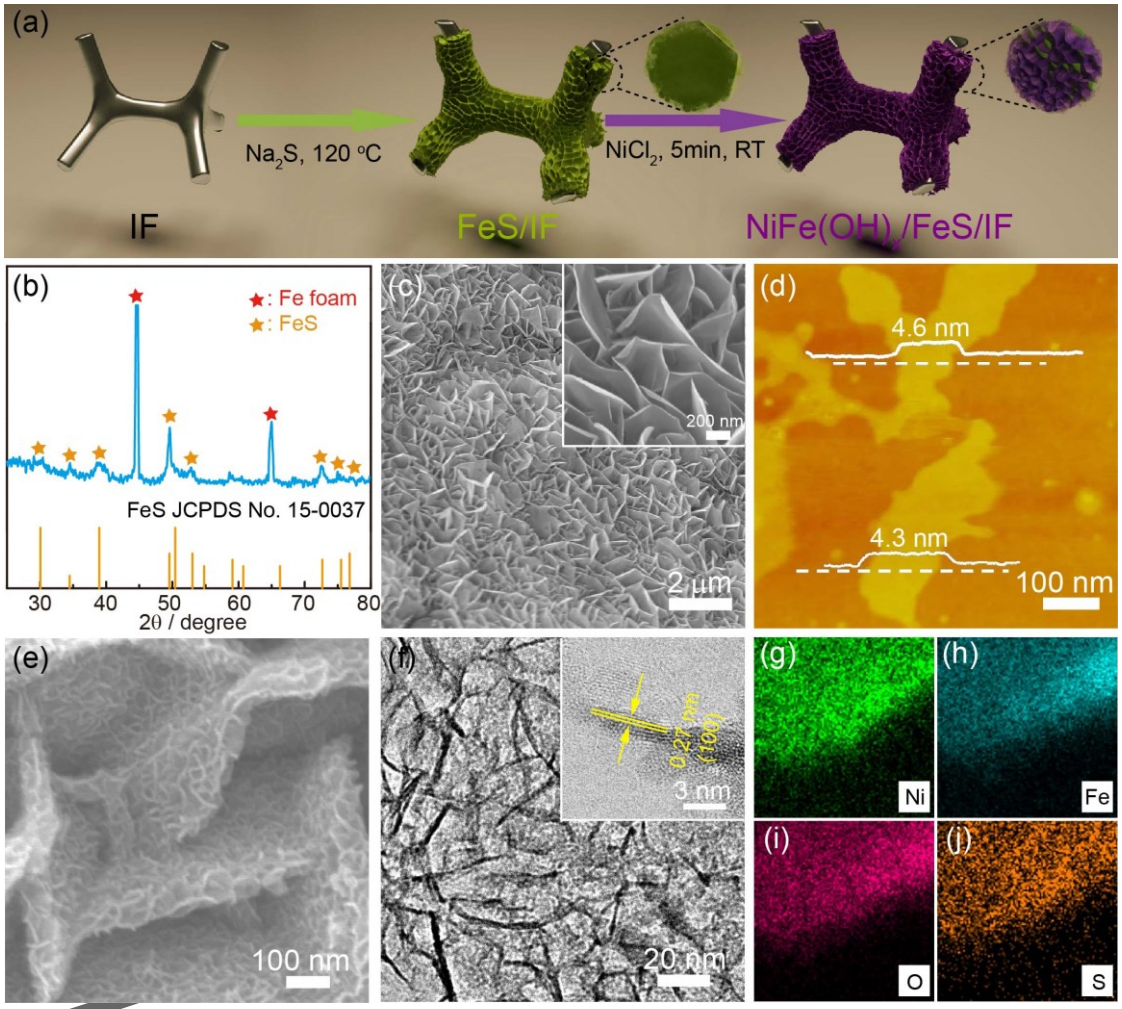

Figure 1. (a) Schematic illustration of the preparation of $NiFe(OH)_x$/FeS/IF. (b) XRD pattern, (c) SEM, and (d) AFM images of FeS/IF. (e) SEM image, (f) TEM image, and (g-j) EDX mapping images of $NiFe(OH)_x$/FeS/IF.

As shown in Figure 1a, $NiFe(OH)_x$/FeS/IF is fabricated by firstly growing ultrathin FeS microsheet arrays using IF as both substrate and Fe source, followed by *in-situ* growing NiFe hydroxides nanosheets on FeS microsheet arrays (see Experimental Section for details). After the first growth, the product was characterized via different techniques. X-ray diffraction (XRD) pattern in Figure 1b shows only diffraction peaks of FeS phase (JCPDS No. 15-0037) at 17.6°, 30.0°, 38.9°, 50.4°, and 76.8° except for the peaks at 44.7° and 65.0° from Fe foam (JCPDS No. 06-0696), indicating the formation

Author

This article is protected by copyright. All rights reserved.

of pure FeS. X-ray photoelectron spectroscopy (XPS) measurement indicates that the product is composed of element Fe and S. In high-resolution Fe 2p spectrum (Figure S1a), the two peaks at binding energies of 707.0 and 710.5 eV are well assigned to Fe^0 and Fe^{2+}, which should originate from IF substrate and FeS microsheets, respectively.[7] In S 2p spectrum (Figure S1b), the peak at 161.8 eV from S^{2-} corroborates the existence of FeS.[7-8] The peak at 168.5 eV can be assigned to oxidized sulfur, which is commonly observed in XPS spectra for metal sulfides upon exposure to air.[7] The morphology of FeS/IF was investigated by scanning electron microscope (SEM). It can be clearly seen that FeS microsheets with a lateral size of serval micrometers are homogeneously grown on IF, as shown in Figure 1c. The thickness of FeS microsheets is determined to be about 4.5 nm by atomic force microscopy (AFM, Figure 1d). The ultrathin nanosheet-like structure is also confirmed in transmission electron microscopic (TEM) image (Figure S2a). High-resolution TEM (HRTEM) image in Figure S2b displays clear lattice fringes with a spacing of 0.29 nm, which agrees with the distance of (101) planes of FeS. The selective area electron diffraction (SAED) pattern further confirms produced microsheet is FeS (Figure S2c). As shown in Figure S3, FeS mackinawite is a 2D materials with high electronic conductivity along its basal planes,[7] enabling it an ideal 3D conductive scaffold for growing other materials.

To integrating highly active $NiFe(OH)_x$ for OER, the as-prepared FeS/IF is simply immersed into Ni^{2+} solution at room temperature (see Experimental Section for details). After reaction for 5 min, the electrode surface becomes much rougher (Figure S4). High-resolution SEM image in Figure 1e clearly shows the successful formation of hierarchical sheet-on-sheet nanostructures. Small nanosheets with a lateral size of about dozens of nanometers are vertically grown on FeS microsheets. TEM image in Figure 1f corroborates a number of vertically aligned nanosheets on larger microsheet. The statistical analysis based on over 50 nanosheets suggests that average thickness of $NiFe(OH)_x$

Author Manuscript

This article is protected by copyright. All rights reserved.

nanosheets is about 3.0 nm. The lattice fringes could be vaguely observed in short range, indicating its low crystallinity (the inset in Figure 1f and Figure S5). The spacing of lattice fringes of 0.27 nm corresponds to the distance of (100) planes of nickel hydroxides, suggesting these nanosheets are hydroxides. XRD pattern (Figure S6) shows the decreased diffraction intensity for FeS due to its partial conversion into hydroxide nanosheets on surface. No obvious new diffraction peaks for hydroxides could be observed, confirming the low crystallinity of nanosheets. The energy dispersive spectroscopic (EDS) mapping results (Figure 1g-j) demonstrate that element Ni, Fe, O, and S are uniformly distributed in the hierarchical sheet-on-sheet nanostructures and their atomic contents are 9.20%, 20.29%, 66.02%, and 4.49% (Figure S7), respectively, indicating Fe-rich composition. Moreover, in order to further understand the formation of $NiFe(OH)_x$/FeS/IF, the reaction process of FeS/IF in Ni^{2+} solution with the reaction time was monitored. In Figure S8a-b, the scattered nanosheets appear on the surface of FeS microsheets since the beginning, meaning the fast nucleation of nanosheets. When the reaction time increases to 5 min, FeS microsheets are entirely covered by the vertical nanosheets (Figure S8c). If keeping increasing the reaction time to 8 min (Figure S8d), the nanosheets keep growing, causing the irregular surface architecture. These observations indicate that reaction time significantly influences the density of $NiFe(OH)_x$ nanosheets on FeS/IF. The optimal reaction time is determined to be 5 min by electrochemical OER tests (Figure S8e-f).

Author Manuscript

This article is protected by copyright. All rights reserved.

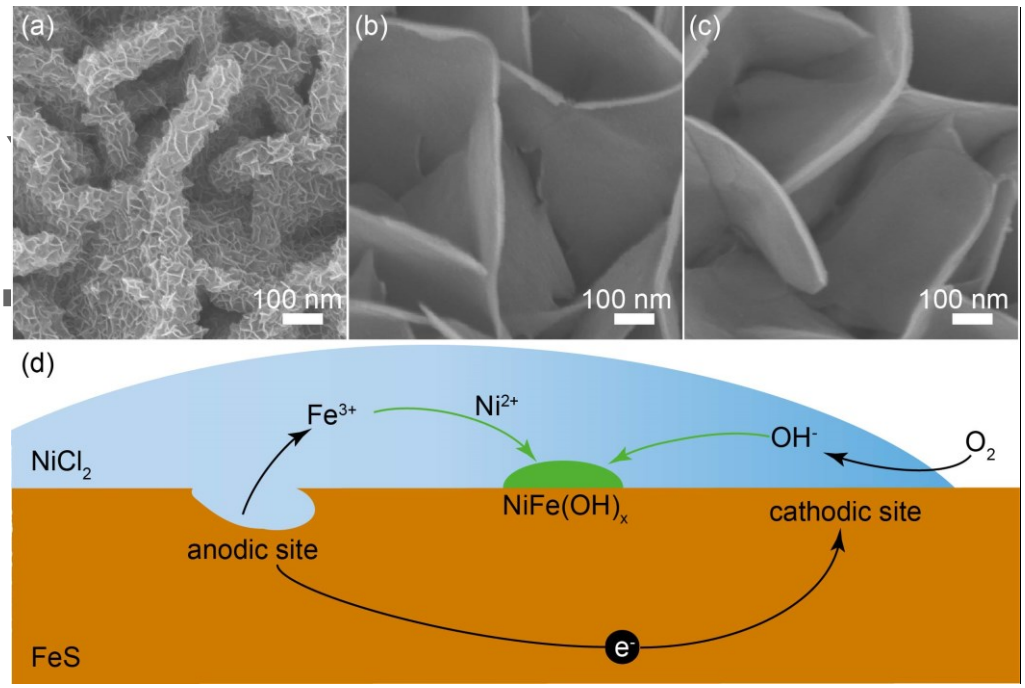

Figure 2. SEM image of the products prepared via the same procedures except for using the following solution instead of $NiCl_2$ solution: (a) $Ni(NO_3)_2$ solution, (b) HCl solution (pH = 5.8), (c) oxygen-removed $NiCl_2$ solution. (d) Schematic illustration of the formation of $NiFe(OH)_x$ nanosheets on FeS/IF.

The formation process of $NiFe(OH)_x$ nanosheets on FeS/IF was explored by conducting the following experiments. Firstly, $Ni(NO_3)_2$ solution was used to replace $NiCl_2$ in the recipe for $NiFe(OH)_x$/FeS/IF. SEM image of the product in Figure 2a shows that similar $NiFe(OH)_x$ nanosheets were grown on FeS/IF, suggesting that Cl^- anion has little effect on the formation of $NiFe(OH)_x$ nanosheets. Secondly, HCl solution (pH is 5.8, same with $NiCl_2$ solution) was used to replace $NiCl_2$. SEM image in Figure 2b reveals that nanosheets were hardly seen on FeS/IF, indicating that Ni^{2+} plays an important role in the formation of $NiFe(OH)_x$ nanosheets. Thirdly, an important control experiment was further conducted by removing the dissolved oxygen in solution. SEM image (Figure 2c) evidences that no nanosheets formed on FeS/IF. This means that the dissolved oxygen participates in the formation of $NiFe(OH)_x$ nanosheets. The above experimental results indicate that

Author Manuscript

This article is protected by copyright. All rights reserved.

the formation of $NiFe(OH)_x$ nanosheets is similar to the corrosion process of iron. Mackinawite FeS is an ionic layered compound with a tetragonal crystal structure (space group P4/nmm, Figure S9a). The layer of tetragonal sheets holds together by van der Waals forces. The Fe atoms form perfect square planar sheets with a Fe-Fe distance of 2.598 Å in FeS (Figure S9b), similar to the Fe-Fe distance in α-Fe (Figure S9c). Due to such very short Fe-Fe distance, the 3d electrons of Fe in FeS are highly delocalized, leading to the strong Fe-Fe metallic bond in the basal planes of FeS.[7, 9] The metallic Fe-Fe bond in FeS is very active and can be easily corroded in the solution with oxygen based on the following thermodynamic equilibrium potential.

$$Fe \rightarrow Fe^{2+} + 2e^- \quad E^\theta = -0.44\ V$$

$$O_2 + 2H_2O + 4e^- \rightarrow 4OH^- \quad E^\theta = 0.40\ V$$

The potential of O_2/OH^- redox is 0.84 V higher than that of Fe^{2+}/Fe redox, indicating metallic iron can be oxidized spontaneously. Therefore, the formation process can be briefly depicted as shown in Figure 2d. Firstly, Fe-Fe bonds in FeS are corroded to produce Fe^{2+} cations and eventually being oxidized to Fe^{3+}. OH^- anions are simultaneously generated from oxygen reduction. Ni^{2+} and in-situ produced Fe^{3+} would compound with OH^- anions to form $NiFe(OH)_x$. To further understand the role of Ni^{2+} in the process, the FeS/IF was also immersed in higher concentration of $NiCl_2$ solution (100 mM). SEM image shows that $NiFe(OH)_x$ nanosheets can be achieved in shorter time (1 min, Figure S10a) than that in 15 mM $NiCl_2$ solution for 5 min. When the reaction time increases to 5 min in 100 mM $NiCl_2$ solution, larger sheet-like structures can be observed (Figure S10b), similar to those obtained in 15 mM $NiCl_2$ solution for 8 min. These results suggest that the higher concentration of $NiCl_2$ solution would accelerate the corrosion of FeS and thus the growth of $NiFe(OH)_x$ nanosheets. It is well known that iron corrosion can be enhanced in salt solution due to the enhanced conductivity

Author Manuscript

This article is protected by copyright. All rights reserved.

of salt solution. Therefore, the presence of Ni^{2+} cations would not only lead to the formation of nanosheet structures but also facilitate the corrosion of metallic iron in the water with oxygen. The corrosion method is a simple, scalable and cost-effective way to access such hierarchically nanostructured materials for multiple applications.

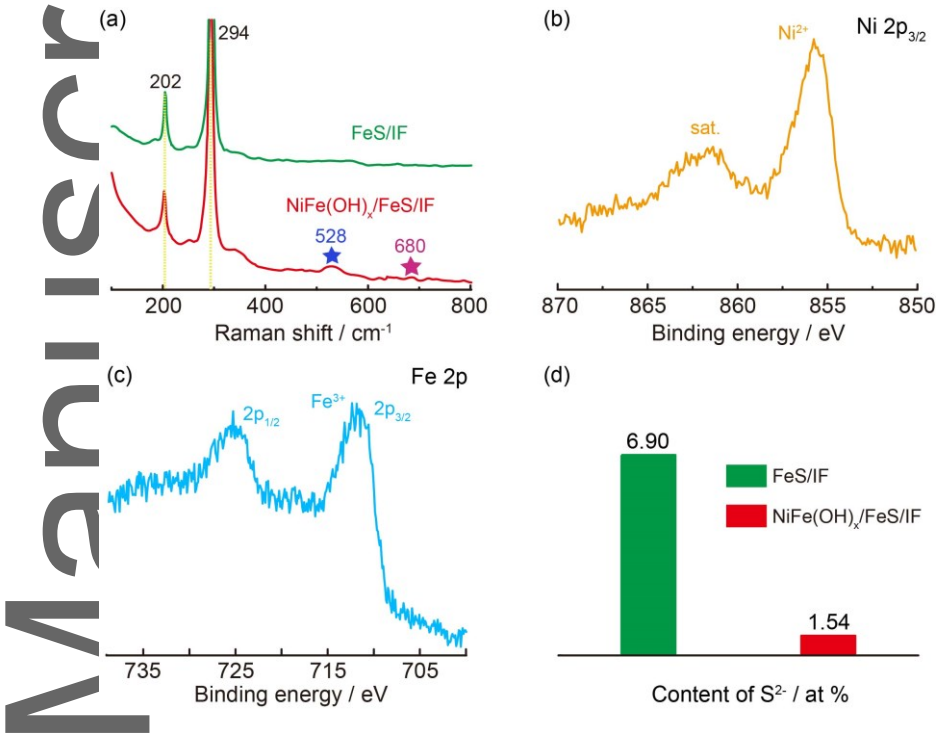

Figure 3. (a) Raman spectra of FeS/IF and $NiFe(OH)_x$/FeS/IF. (b) Ni $2p_{3/2}$ and (c) Fe 2p XPS spectra of as-prepared $NiFe(OH)_x$/FeS/IF. (d) Content of S^{2-} in metal sulfides for FeS/IF and $NiFe(OH)_x$/FeS/IF from S 2p spectra.

Raman spectroscopy was used to further analyze the composition of $NiFe(OH)_x$/FeS/IF. As shown in Figure 3a, all the peaks at 202, and 294 cm^{-1} observed in FeS/IF are the characteristic Raman vibration of FeS.[9a] Except for those peaks, a peak at 528 cm^{-1} is detected for $NiFe(OH)_x$/FeS/IF, which should come from Ni-O vibrations of $Ni(OH)_2$ clusters according to the reported value of 532 cm^{-1} for the defective or disordered $Ni(OH)_2$.[10] Another peak at 680 cm^{-1} can be attributed to the Fe-

Author Manuscript

This article is protected by copyright. All rights reserved.

O vibrations.[11] The above evidences corroborate the formation of $NiFe(OH)_x$ on FeS nanosheets. The elemental chemical states in $NiFe(OH)_x$/FeS/IF were further studied by XPS. The Ni 2p3/2 spectrum shows a typical peak of Ni^{2+} species at 855.8 eV, accompanied by a satellite peak at 862.2 eV (Figure 3b).[12] The two main Fe 2p peak at 711.7 and 725.1 eV are the typical peaks of Fe^{3+},[13] indicating it is the dominant chemical state of Fe on the surface of $NiFe(OH)_x$/FeS/IF (Figure 3c). The atomic ratio of Ni to Fe is determined to be about 1.23 from XPS results. Besides, the atomic content of S^{2-} from metal sulfides in deconvoluted S 2p spectra (Figure S11) decreases from 6.90% for FeS/IF to 1.54% for $NiFe(OH)_x$/FeS/IF (Figure 3d). This should be due to the S loss during the partial conversion of FeS into $NiFe(OH)_x$ nanosheets and the cover of $NiFe(OH)_x$ on FeS. Above results demonstrate the successful construction of hierarchical sheet-on-sheet $NiFe(OH)_x$/FeS/IF structure via a facile method, which would not only provide a sufficient amount of highly-active and accessible sites for OER from bimetallic $NiFe(OH)_x$, but also guarantee the efficient electron/mass transfer from conductive microporous FeS/IF scaffold. In order to give more solid evidence on the formation of $NiFe(OH)_x$ nanosheets, phase-pure FeS powder was also prepared and used it for the growth of $NiFe(OH)_x$ nanosheets. As shown in Figure S12, a series of characterizations corroborate the formation of $NiFe(OH)_x$ on FeS (see Supporting Information for details).

Author Manuscript

This article is protected by copyright. All rights reserved.

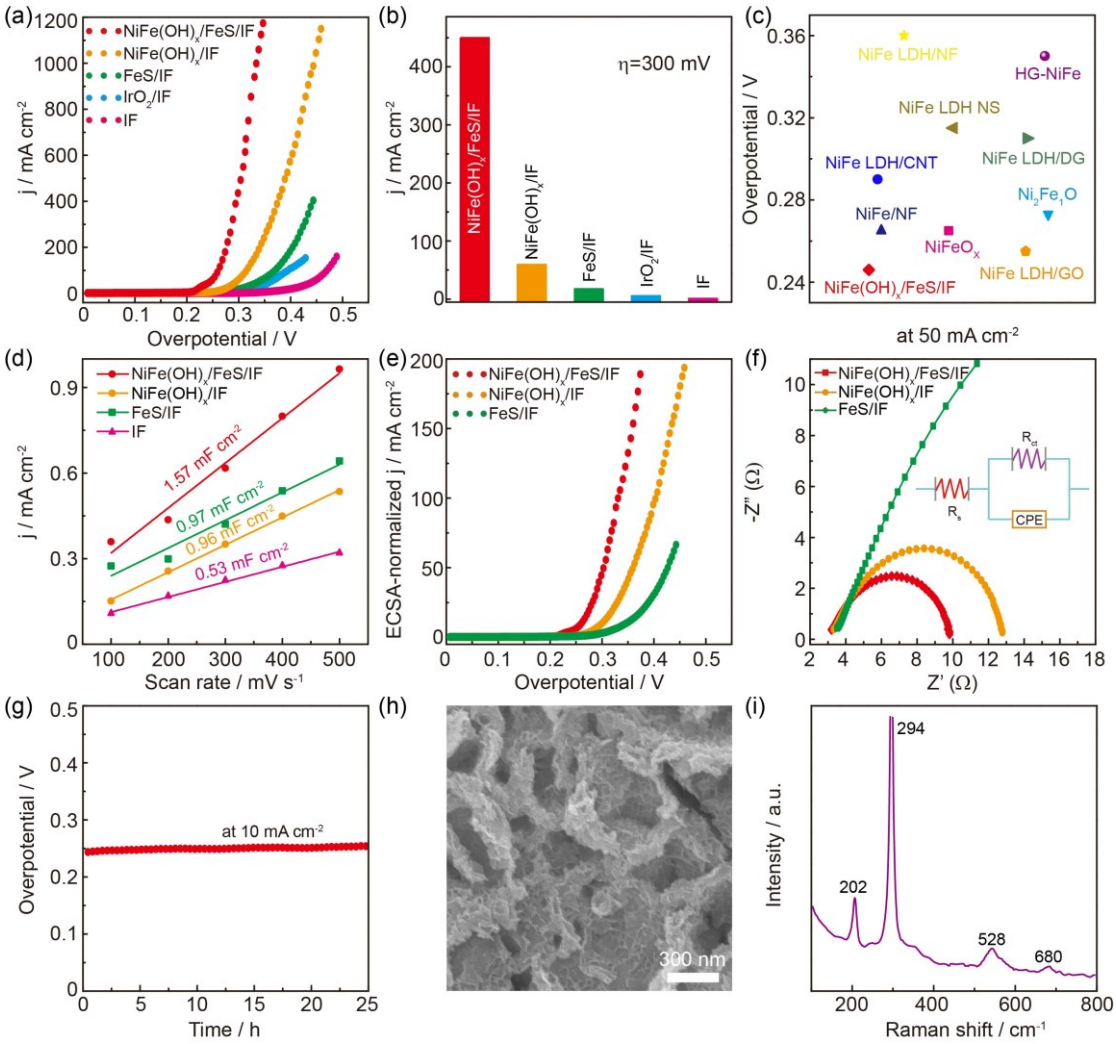

Figure 4. (a) LSV curves of as-prepared catalysts at scan rate of 2 mV s^{-1} with 85% iR-compensation. (b) A comparison of current density at η = 300 mV for the prepared catalysts. (c) A comparison of overpotentials at 50 mA cm^{-2} for $NiFe(OH)_x/FeS/IF$ and reported analogous catalysts. (d) Current density as a function of scan rate, (e) ECSA-normalized LSV curves, and (f) Nyquist plots of as-prepared catalysts. (g) Chronopotentiometric curve recorded on $NiFe(OH)_x/FeS/IF$ at a constant current density of 10 mA cm^{-2}. (h) SEM image and (i) Raman spectra of $NiFe(OH)_x/FeS/IF$ after OER durability test.

The electrocatalytic activity of as-prepared catalysts for OER was firstly evaluated by linear scan voltammetry (LSV) using a typical three-electrode system with a scan rate of 2 mV s^{-1} in 1.0 M KOH electrolyte. All the overpotentials were given with 85% iR-compensation unless specified.

Author

This article is protected by copyright. All rights reserved.

Commercial IrO_2 nanoparticles supported on IF (denoted as IrO_2/IF) was also used for comparison. As shown in Figure 4a and Figure S13, FeS/IF exhibits good catalytic activity with a low overpotential of 339 mV at 50 mA cm^{-2}, 23 mV and 104 mV lower than IrO_2/IF and bare IF, respectively. However, both electrodes could not stably output the large current density such as over 500 mA cm^{-2}, although it is necessary for practical operation of water splitting in industry. In contrast, $NiFe(OH)_x$/FeS/IF exhibits significantly enhanced OER performance. The overpotential decreases to 245 mV at 50 mA cm^{-2}, 94 mV lower than FeS/IF, which indicates $NiFe(OH)_x$ nanosheets in-situ grown on FeS microsheets should be responsible for the improved OER activity. Notably, this hierarchical nano/micro sheet-on-sheet nanostructured electrode can steadily output high current densities of 500 and 1000 mA cm^{-2} at low overpotentials of 304 and 332 mV, respectively, without appreciable interference by intensively evolved O_2 bubbles. It can be seen that bare IF shows very poor activity for OER compared with $NiFe(OH)_x$/FeS/IF, indicating the contribution of iron substrate to the overall OER current can be negligible. Moreover, to investigate the contribution of FeS nanosheet arrays to the superior catalytic activity of $NiFe(OH)_x$/FeS/IF, bare IF without pre-grown FeS microsheets was used to react in Ni^{2+} aqueous solution at room-temperature. $NiFe(OH)_x$ nanosheet arrays could be grown on IF (denoted as $NiFe(OH)_x$/IF) as evidenced by SEM, TEM, HRTEM, and elemental mapping (Figure S14-S16). As shown in Figure 4a, $NiFe(OH)_x$/IF shows an overpotential of 295 mV at 50 mA cm^{-2} and can steadily output the current density of 500 and 1000 mA cm^{-2} at overpotentials of 390 and 445 mV, respectively. Such activity is much better than FeS/IF and IrO_2/IF, but still appreciably lower than that for $NiFe(OH)_x$/FeS/IF. The current density at the overpotential of 300 mV for all prepared catalysts are compared in Figure 4b. It can be clearly seen that $NiFe(OH)_x$/FeS/IF delivers a current density of 450 mA cm^{-2}, which is about 7.5, 25, 75, and 450 times higher than $NiFe(OH)_x$/IF (60 mA cm^{-2}), FeS/IF (18 mA cm^{-2}), IrO_2/IF (6 mA cm^{-2}), and IF (1 mA cm^{-2}), respectively. These results

Author Manuscript

This article is protected by copyright. All rights reserved.

demonstrate that the strategy using FeS nanosheet as scaffold to fabricate hierarchical nano/micro sheet-on-sheet nanostructured $NiFe(OH)_x$/FeS/IF is very effective to boost OER activity, especially at larger current output. The performance is appreciably better than reported NiFe hydroxide-based analogues and other non-precious OER electrocatalysts (Figure 4c and Table S1) in 1 M KOH, such as NiFe/NF, NiFe LDH/CNT/CF (η_{50}=290 mV),[14] Ni_2Fe_1O (η_{50}=273 mV),[12c] $NiFeO_x$/CFP (η_{50}=265 mV),[15] NiFe LDH/DG (η_{50}=310 mV),[16] NiFe LDH/GO (η_{50}=255 mV),[17] S-$NiFe_2O_4$/Ni_3Fe/NW (η_{50}=253 mV),[18] and HG-NiFe (η_{50}=350 mV).[19] The Faradaic efficiency of $NiFe(OH)_x$/FeS/IF for OER was calculated to be 96.7% (Figure S17).

In order to further understand the origin of high activity of $NiFe(OH)_x$/FeS/IF, the electrochemical surface areas (ECSA) of as-prepared catalysts were evaluated by measuring double-layer capacitance (C_{dl}) which is directly correlated with ECSA (Figure S18 and Figure 4d). The C_{dl} of $NiFe(OH)_x$/FeS/IF is 1.57 mF cm^{-2}, which is 1.6 times higher than FeS/IF (0.97 mF cm^{-2}) and $NiFe(OH)_x$/IF (0.96 mF cm^{-2}). Such increase cannot account for the 25-fold activity enhancement from FeS/IF to $NiFe(OH)_x$/FeS/IF and 7.5-fold activity enhancement from $NiFe(OH)_x$/IF to $NiFe(OH)_x$/FeS/IF. Accordingly, the OER current densities were further normalized by ECSA as shown in Figure 4e (see Experimental Section for details). The $NiFe(OH)_x$/FeS/IF still greatly outperforms $NiFe(OH)_x$/IF and FeS/IF, suggesting that the $NiFe(OH)_x$ is the real active sites of the catalyst. The synergistic effect between $NiFe(OH)_x$ and FeS contributes to the superior OER activity of $NiFe(OH)_x$/FeS/IF besides the increase of ECSA. Furthermore, electrochemical impedance spectroscopy (EIS) technique was used to investigate the electron transfer kinetics during the OER process. All Nyquist plots were fitted to equivalent circuit. In Figure 4f, all as-prepared catalysts exhibit similar solution resistance (R_s) of about 3.3 Ω, but a significantly distinct charge transfer resistances (R_{ct}). The $NiFe(OH)_x$/FeS/IF electrode shows the smallest R_{ct} value of about 6.8 Ω compared with the values of 9.6 Ω for $NiFe(OH)_x$/IF and 41.6 Ω for

Author Manuscript

This article is protected by copyright. All rights reserved.

FeS/IF, indicating the fastest electron transfer kinetics of OER on $NiFe(OH)_x$/FeS/IF. Therefore, the high intrinsic activity of NiFe bimetallic hydroxides, conductive FeS microsheet scaffold, and hierarchical nano/micro sheet-on-sheet electrode architecture with abundant accessible active sites should synergistically contribute to the boosted OER activity of hybrid $NiFe(OH)_x$/FeS/IF.

Besides the catalytic activity, the durability of $NiFe(OH)_x$/FeS/IF was firstly tested by chronopotentiometric measurement at a constant current density of 10 mA cm^{-2}. The overpotential did not increase after 25 h test (Figure 4g). The morphology and Raman spectra of $NiFe(OH)_x$/FeS/IF after long-term stability test were recorded. As shown in Figure 4h, the hierarchical nano/micro sheet-on-sheet nanostructure is well maintained. The typical peaks of FeS and $NiFe(OH)_x$ in Raman spectrum suggest that $NiFe(OH)_x$/FeS/IF catalyst is robust for water oxidation (Figure 4i). Furthermore, the durability of $NiFe(OH)_x$/FeS/IF was checked by continuous potential cycling between 1.12 and 1.67 V for 500 cycles and the result was shown in Figure S19. The current density can reach as high as about 300 mA cm^{-2}. It can be seen that the CV after 500 cycles almost overlaps with the initial one, further confirming the good stability of as-preapred $NiFe(OH)_x$/FeS/IF. These experiments indicate the excellent durability of $NiFe(OH)_x$/FeS/IF electrode, which should be ascribed to the in-situ growth of robust FeS microsheets on IF and the in-situ formation of $NiFe(OH)_x$ nanosheets on FeS microsheet. Such nano/micro sheet-on-sheet architecture also provide a superhydrophilic surface (as proved by a contact-angle measurement shown in Figure S20 and Movie S1) to enable the prompt gas release, avoiding the issues of mechanical peel-off of catalysts and block of catalytic sites during gas evolution.

Such excellent OER performance inspires us to assemble a water-alkali electrolyzer to evaluate the potential of $NiFe(OH)_x$/FeS/IF electrode for overall water splitting. A previously reported $MoNi_4$ on MoO_2 cuboids (denoted as $MoNi_4/MoO_2$/NF) was synthesized (see Experimental section for details)

This article is protected by copyright. All rights reserved.

Author Manuscript

according to the literature as the cathode for hydrogen evolution reaction (HER).[20] As shown in Figure 5a, the as-prepared $MoNi_4/MoO_2$/NF requires a very low overpotential of 15 mV at 10 mA cm^{-2} for HER. A two-electrode water electrolyzer was subsequently assembled using $NiFe(OH)_x$/FeS/IF as anode and $MoNi_4/MoO_2$/NF as cathode. The optical photograph (inset in Figure 5b) and a video (Movie

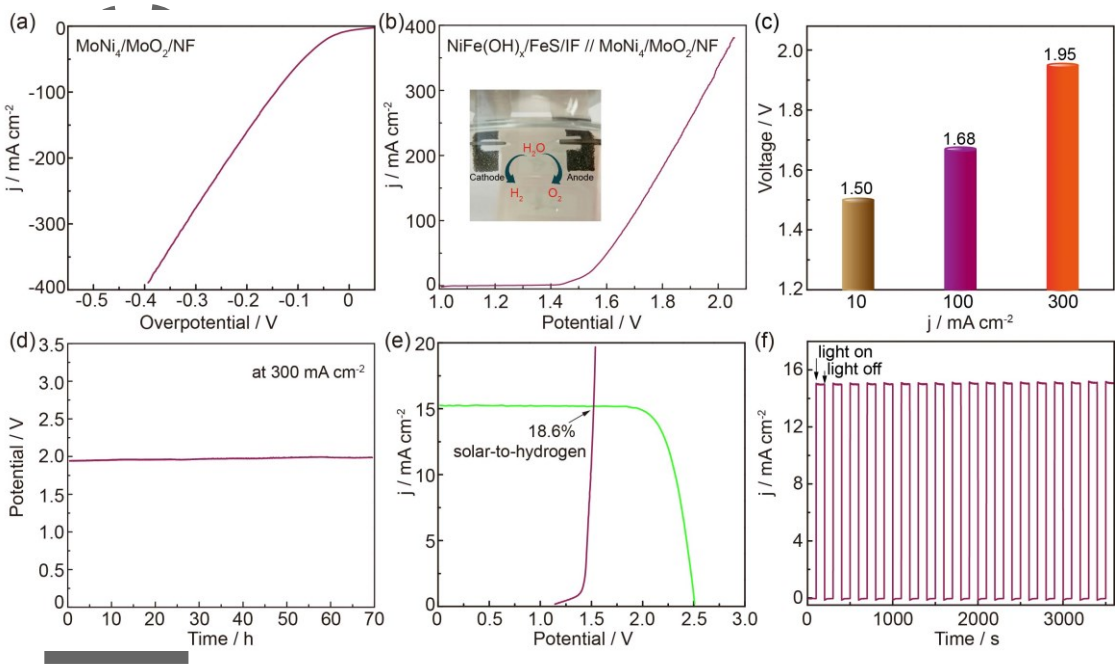

Figure 5. (a) LSV polarization curves of $MoNi_4/MoO_2$/NF for HER at a scan rate 2 mV s^{-1} without iR-compensation. (b) LSV polarization curve of overall water splitting electrolyzer composed of $MoNi_4/MoO_2$/NF as cathode and $NiFe(OH)_x$/FeS/IF as anode. The inset is an optical photograph of the water splitting electrolyzer. (c) Cell voltage of overall water splitting electrolyzer at different current densities. (d) Long-term durability of overall water splitting at a current density of 300 mA cm^{-2}. (e) J-V curves under simulated AM 1.5G 100 mW cm^{-2} illumination for GaAs cell integrated with overall water splitting. (f) Current density against time under chopped illumination of photo-assisted water splitting device without external bias.

Author Manuscript

This article is protected by copyright. All rights reserved.

S2) taken during the operation suggests the electrolyzer can stably operate with rapid gas evolution. The polarization curve of overall water splitting gives a very small cell voltage of 1.50 V at a current density of 10 mA cm^{-2}, 1.68 V at 100 mA cm^{-2} and 1.95 V at 300 mA cm^{-2} (Figure 5b-c), which is impressive and outperforms most of the recent state-of-the-art materials (Table S2). The durability for overall water splitting was evaluated at a large current density of 300 mA cm^{-2}. It can be seen from Figure 5d that the cell voltage shows negligible loss even after test for 70 h, suggesting its superior operational durability. Such activity and durability of the present $NiFe(OH)_x$/FeS/IF demonstrate its promising potential in a practical electrolyzer. Furthermore, such water splitting electrolyzer was integrated with a commercial GaAs solar cell to construct a photo-assisted water splitting system under AM 1.5G (Figure 5e). The solar-to-hydrogen efficiency of such system is calculated to be up to 18.6% with continuous hydrogen and oxygen bubbles released. Moreover, the photocurrent does not show decay after 3600 seconds duration (Figure 5f), demonstrating the potential application of the present catalyst in a practical unbiased photo-assisted water splitting system.

Lastly, it should be noted that the developed synthetic strategy could work as a general method for preparing other bimetallic or multimetallic $MFe(OH)_x$/FeS/IF. A series of $MFe(OH)_x$/FeS/IF (for example, M = Co, V, Cr etc.) can be easily prepared by simply replacing Ni^{2+} solution with the corresponding Co^{2+}, V^{3+}, and Cr^{3+} aqueous solution and immersing pre-grown FeS/IF electrode into the solution for a couple of minutes at room temperature. The obtained products were denoted as $CoFe(OH)_x$/FeS/IF, $VFe(OH)_x$/FeS/IF, and $CrFe(OH)_x$/FeS/IF, respectively. As seen in Figure S21a-c, nano/micro sheets-on-sheets hybrid nanostructures were also formed for above three catalysts, indicating the versatility of the present strategy. Furthermore, signals about Co, Cr, and V can be clearly observed, indicating the successful introduction of Co, Cr, and V in $CoFe(OH)_x$/FeS/IF,

This article is protected by copyright. All rights reserved.

Author Manuscript

$CrFe(OH)_x$/FeS/IF, and $VFe(OH)_x$/FeS/IF, respectively. (Figure S22). The OER catalytic activities were also evaluated and compared with $NiFe(OH)_x$/FeS/IF as shown in Figure S21d and S21e. $CrFe(OH)_x$/FeS/IF shows the worst OER activity with an overpotential of 380 mV at 100 mA cm^{-2}, slightly larger than 359 mV on $VFe(OH)_x$/FeS/IF. This performance is comparable to bare FeS/IF (overpotential of 370 mV at 100 mA cm^{-2}), suggesting that Cr and V ion may not be suitable candidates to improve OER activity of metal hydroxides although they may work for other electrochemical applications. In contrast, the overpotential at 100 mA cm^{-2} significantly decrease to 306 mV on $CoFe(OH)_x$/FeS/IF and further down to 261 mV on $NiFe(OH)_x$/FeS/IF, indicating Co or Ni doping is effective for boosting OER activity of $Fe(OH)_x$ and Ni is best. These results demonstrate that the present facile and scalable strategy is capable of producing a series of bimetallic hydroxides to screen highly efficient catalysts for OER or other applications.

In summary, by taking into account the requirements for a practical water oxidation electrode, we demonstrate here that using ultrathin conductive FeS microsheets pre-grown on iron foam as 3D microporous conductive scaffold to *in-situ* integrate vertical bimetallic $NiFe(OH)_x$ nanosheet arrays is an effective strategy for fabricating highly efficient OER electrode. The hierarchical nano/micro sheet-on-sheet structure and the hybrid composition of $NiFe(OH)_x$ and FeS are investigated by systematic characterizations. The electrochemical measurements indicate that integrating $NiFe(OH)_x$ nanosheet arrays on conductive FeS microsheet arrays significantly boosts the OER activity. Benefiting from the hierarchical nano/micro electrode architecture for abundant catalytic sites, efficient electron/mass transfer, and prompt gas release, the prepared $NiFe(OH)_x$/FeS/IF electrode not only exhibits low overpotentials of 245 mV at 50 mA cm^{-2} and 261 mV at 100 mA cm^{-2}, but also can steadily output high current density of 500 and 1000 mA cm^{-2} at a low overpotential of 304 and 332 mV, respectively. A water-alkali electrolyzer using $NiFe(OH)_x$/FeS/IF as anode and

Author Manuscript

This article is protected by copyright. All rights reserved.

$MoNi_4/MoO_2$/NF as cathode demonstrates the continuous hydrogen production at a high output of 300 mA cm^{-2} with a small cell voltage. The lost-cost Fe-based catalyst materials and cost-effective facile preparation for mass production enable its potential application in practical water splitting. These results open up an avenue for the rational design of low cost, highly active and practical electrocatalysts for diverse applications.

Experimental Section

Chemicals: All reagents were of analytical grade and used without further purification. Iron foam (labeled as IF) and nickel foam (labeled as NF) were purchased from Kunshan Kuangxun Electrical Co., Ltd. Sodium sulfide nonahydrate was purchased from Acros Organics. Nickel(II) chloride hexahydrate, vanadium(III) chloride, cobalt(II) chloride hexahydrate, chromium(III) chloride hexahydrate, ammonium molybdate tetrahydrate, nickel nitrate hexahydrate and commercial IrO_2 nanoparticles were obtained from Alfa Aesar. Ethanol and acetone were purchased from Beijing Chemical Works. Milli-Q deionized water (resistance of 18.2 MΩ·cm at 25 ^oC) were used for all experiments.

Preparation of FeS/IF: IF (20 mm x 30 mm, 1.9 mm in thickness) was ultrasonically cleaned in ethanol, acetone, and deionized water for 30 min prior to use. For the preparation of FeS/IF, a piece of pretreated IF was placed in a Teflon lined stainless autoclave (25 mL) containing 15 mL of 0.3 M $Na_2S·9H_2O$ aqueous solution. The autoclave was sealed and maintained at 120 ^oC for 12 h in an electric oven. After the autoclave cooled down slowly to room temperature, the sample was taken out and washed with water and ethanol thoroughly before drying.

Author Manuscript

This article is protected by copyright. All rights reserved.

Preparation of NiFe(OH)$_x$/FeS/IF: For the preparation of corrosive solution, 0.375 mmol of $NiCl_2 \cdot 6H_2O$ was added into 25 mL deionized water to make a transparent Ni^{2+} solution in a beaker. The pH of the aqueous solution containing $NiCl_2 \cdot 6H_2O$ is 5.8, and then a piece of as-prepared FeS/IF was immersed into 25 mL nickel chloride solution (15 mM) and maintained at room temperature for 5 min. After that, it was taken out and washed with water and ethanol for several times and dried at room temperature for use. The loading of NiFe(OH)$_x$/FeS on iron foam and NiFe(OH)$_x$ on FeS/IF are estimated to be about 5.2 and 0.4 mg cm^{-2}, respectively.

Preparation of other MFe(OH)$_x$/FeS/IF: A series of MFe(OH)$_x$/FeS/IF (M=V, Co, Cr) were prepared according to the same protocol as that for NiFe(OH)$_x$/FeS/IF except for using the same amount of corresponding metal salts to replace nickel chloride solution. Specifically, vanadium chloride, cobalt chloride hexahydrate, and chromium chloride hexahydrate were used for the synthesis of VFe(OH)$_x$/FeS/IF, CoFe(OH)$_x$/FeS/IF, and CrFe(OH)$_x$/FeS/IF, respectively.

Preparation of NiFe(OH)$_x$/IF: A piece of IF was immersed into 25 mL nickel chloride solution (15 mM) and maintained at room temperature for 5 min. After that, it was taken out and washed with water and ethanol several times and dried at room temperature for use.

Preparation of MoNi$_4$/MoO$_2$/NF: A piece of nickel foam (10 mm x 30 mm, 1.9 mm in thickness) was ultrasonically cleaned in ethanol, acetone, and deionized water for 30 min prior to use. According to previously reported method,[20] a piece of pretreated nickel foam was immersed into 15 mL of H_2O containing 0.04 M $Ni(NO_3)_2 \cdot 6H_2O$ and 0.01 M $(NH_4)_6Mo_7O_{24} \cdot 6H_2O$ in a Teflon autoclave. The autoclave was sealed and maintained at 150 ^oC for 6 h in an electric oven. After washing with deionized water, the $NiMoO_4$ cuboids were achieved on the nickel foam. Finally, the as-constructed

Author Manuscript

This article is protected by copyright. All rights reserved.

$NiMoO_4$ cuboids were heated at 500 °C for 2 h in a H_2/Ar (v./v., 10/90) atmosphere, and then, the $MoNi_4$ electrocatalyst anchored on the MoO_2 cuboids was obtained.

Characterizations

The field-emission scanning electron microscopy (SEM) images were taken on a Hitachi S-4800 at an acceleration voltage of 15 kV. The transmission electron microscopy (TEM) and corresponding elemental distribution analyses were performed on a JEM-2100F equipped with energy dispersive X-ray spectrometer, working on an acceleration voltage of 200 kV. Atomic force microscopy (AFM) image was taken on a Bruker Dimension Icon microscope. For AFM measurement, the samples were peel-off Fe foam and dipped on Si substrate without any additional treatment. The surface elemental information was obtained by X-ray photoelectron spectroscopy (XPS) performed on the Thermo Scientific ESCALab 250Xi using 200 W monochromated Al Kα radiation. The binding energies for all spectra were calibrated with respect to C 1s line at 284.8 eV. Powder X-ray diffraction (XRD) patterns were recorded on a Regaku D/Max-2500 diffractometer equipped with a Cu Kα1 radiation (λ=1.54056 Å). The Raman spectra were recorded using a LabRAM HR Evolution spectroscope (HORIBA, France).

Electrochemical Measurements

Oxygen evolution reaction (OER) and hydrogen evolving reaction (HER). All electrochemical measurements were carried out with an electrochemical workstation Autolab PGSTAT 302N (Metrohm, The Netherlands). Using a conventional three-electrode cell in 1.0 M KOH electrolyte. The as-prepared electrodes, Hg/HgO electrode (1 M KOH), and carbon rod were used as working electrode, reference electrode, and counter electrode, respectively.

Author Manuscript

This article is protected by copyright. All rights reserved.

All measured potentials were converted to the reversible hydrogen electrode (RHE), according to the equation:

$$E_{RHE}=E_{Hg/HgO}+0.098+0.059*pH$$

The linear sweep voltammetry (LSV) curves were recorded at a scan rate of 2 mV s^{-1}. All curves were recorded with 85% iR-compensation unless specified. The long-term durability test was performed using chronopotentiometry method at a constant current density. The C_{dl} values for as-prepared working electrodes were determined from the cyclic voltammogram (CV) in the double layer region (without faradaic processes) at different scan rates. Electrochemical impedance spectroscopy (EIS) was carried out with a frequency range from 100 KHz to 0.01 Hz and an amplitude of 5 mV.

ECSA-normalized LSV curves. For the purpose of excluding the improvement by ECSA, the OER performance was normalized by ECSA. The ECSA-normalized current density for as-prepared catalysts was calculated to be:

$$\text{ECSA-normalized current density} = \text{current density}*C_s/C_{dl}$$

C_s is the specific capacitance. In this work, 0.040 mF cm^{-2} was adopted as the value of C_s based on previously reported OER catalysts in alkaline solution.[21]

Overall water splitting. Overall water splitting measurement was performed in a two-electrode system consisting of $NiFe(OH)_x$/FeS/IF as anode electrode and $MoNi_4/MoO_2$/NF as cathode electrode. The LSV curve for overall water splitting was recorded in 1.0 M KOH at a rate 2 mV s^{-1} without iR-compensation.

Calculation for Faradaic efficiency

Author Manuscript

This article is protected by copyright. All rights reserved.

Electrolysis was performed under a constant applied current density of 100 mA cm^{-2} in a custom-built H-type cell in which the auxiliary electrode (carbon rod) is placed in one compartment while the reference (Ag/AgCl) and working electrode are placed in another. The product was subsequently detected by a thermal conductivity detector (TCD) in Agilient 7890B gas chromatography (GC). Helium was used as a carrier gas. Atmospheric nitrogen was used as an internal standard. The Faradaic efficiency was obtained by comparing the theoretical amount of oxygen that should be produced based on the charge consumption to the amount of oxygen determined using gas chromatography. The Faradaic efficiency was calculated by the following equation:

$$FE\% = 4nF/Q$$

Where F and n are the faraday constant and the amount of produced oxygen, respectively; Q is the total amount of charge flowed past the electrochemical cell.

Supporting Information

Supporting Information is available from the Wiley Online Library or from the author.

Acknowledgements

S. Niu and W.-J. Jiang contributed equally to this work. We acknowledge the financial support from the National Key Research and Development Program of China (2016YFB0101202), the National Natural Science Foundation of China (21773263, 91645123 and 21573249), the Strategic Priority Research Program of the Chinese Academy of Sciences (XDB12020100), the National Postdoctoral Program for Innovative Talents (BX2001700250), and the project funded by China Postdoctoral Science Foundation (2017M620912). We thank Dr. Fen Liu, Dr. Zhijuan Zhao, Xiaoyu Zhang for their help in XPS analysis; Yang Sun for XRD analysis; and Dr. Bo Guan and Ji-Ling Yue for SEM experiments.

Author Manuscript

This article is protected by copyright. All rights reserved.

Received: ((will be filled in by the editorial staff))
Revised: ((will be filled in by the editorial staff))
Published online: ((will be filled in by the editorial staff))

References

[1] a) J. Li, Y. Wang, T. Zhou, H. Zhang, X. Sun, J. Tang, L. Zhang, A. M. Alenizi, Z. Yang, G. Zheng, *J. Am. Chem. Soc.* **2015**, 137, 14305; b) C. G. Moralesguio, L. Liardet, X. Hu, *J. Am. Chem. Soc.* **2016**, 138, 8946; c) Y. Zhao, R. Nakamura, K. Kamiya, S. Nakanishi, K. Hashimoto, *Nat. Commun.* **2013**, 4, 2390.

[2] a) Z. Xiao, Y. Wang, Y.-C. Huang, Z. Wei, C.-L. Dong, J. Ma, S. Shen, Y. Li, S. Wang, *Energy Environ. Sci.* **2017**, 10, 2563; b) T. Tang, W.-J. Jiang, S. Niu, N. Liu, H. Luo, Y.-Y. Chen, S.-F. Jin, F. Gao, L.-J. Wan, J.-S. Hu, *J. Am. Chem. Soc.* **2017**, 139, 8320; c) C. Tang, H. Wang, H. Wang, Q. Zhang, G. Tian, J. Nie, F. Wei, *Adv. Mater.* **2015**, 27, 4524; d) Y. P. Zhu, T. Ma, M. Jaroniec, S. Z. Qiao, *Angew. Chem. Int. Ed.* **2017**, 56, 1324; e) K. Xu, H. Ding, K. Jia, X. Lu, P. Chen, T. Zhou, H. Cheng, S. Liu, C. Wu, Y. Xie, *Angew. Chem. Int. Ed.* **2016**, 55, 1710; f) T. Wang, G. Nam, Y. Jin, X. Wang, P. Ren, M. G. Kim, J. Liang, X. Wen, H. Jang, J. Han, Y. Huang, Q. Li, J. Cho, *Adv. Mater.* **2018**, 30, 1800757.

[3] a) L. Trotochaud, S. L. Young, J. K. Ranney, S. W. Boettcher, *J. Am. Chem. Soc.* **2014**, 136, 6744; b) J. Y. Chen, L. Dang, H. Liang, W. Bi, J. B. Gerken, S. Jin, E. E. Alp, S. S. Stahl, *J. Am. Chem. Soc.* **2015**, 137, 15090; c) Y. Liu, X. Liang, L. Gu, Y. Zhang, G.-D. Li, X. Zou, J.-S. Chen, *Nat. Commun.* **2018**, 9, 2609.

[4] a) D. K. Zhong, J. Sun, H. Inumaru, D. R. Gamelin, *J. Am. Chem. Soc.* **2009**, 131, 6086; b) X. Lu, C. Zhao, *Nat. Commun.* **2015**, 6, 6616.

Author Manuscript

This article is protected by copyright. All rights reserved.

[5] a) C. Tang, N. Cheng, Z. Pu, W. Xing, X. Sun, *Angew. Chem. Int. Ed.* **2015**, 127, 9483; b) Y. Wu, Y. Liu, G.-D. Li, X. Zou, X. Lian, D. Wang, L. Sun, T. Asefa, X. Zou, *Nano Energy* **2017**, 35, 161; c) S. Niu, W. J. Jiang, T. Tang, Y. Zhang, J. H. Li, J. S. Hu, *Adv. Sci.* **2017**, 4, 1700084; d) T. Tang, W. J. Jiang, S. Niu, J. S. Hu, *J. Electrochem.* **2018**, 24, 409.

[6] a) C.-L. Sun, B.-J. Li, Z.-J. Shi, *Chem. Rev.* **2011**, 111, 1293; b) S. Enthaler, K. Junge, M. Beller, *Angew. Chem. Int. Ed.* **2008**, 47, 3317.

[7] X. Zou, Y. Wu, Y. Liu, D. Liu, W. Li, L. Gu, H. Liu, P. Wang, L. Sun, Y. Zhang, *Chem* **2018**, 4, 1139.

[8] a) J. Jiang, S. Lu, H. Gao, X. Zhang, H.-Q. Yu, *Nano Energy* **2016**, 27, 526; b) X. Ren, W. Wang, R. Ge, S. Hao, F. Qu, G. Du, A. M. Asiri, Q. Wei, L. Chen, X. Sun, *Chem. Commun.* **2017**, 53, 9000.

[9] a) L. M. White, R. Bhartia, G. D. Stucky, I. Kanik, M. J. Russell, *Earth Planet. Sci. Lett.* **2015**, 430, 105; b) D. Rickard, G. W. Luther, *Chem. Rev.* **2007**, 107, 514; c) K. D. Kwon, K. Refson, S. Bone, R. Qiao, W. Yang, Z. Liu, G. Sposito, *Phys. Rev. B* **2011**, 83, 064402.

[10] J. Yan, W. Sun, T. Wei, Q. Zhang, Z. Fan, F. Wei, *J. Mater. Chem.* **2012**, 22, 11494.

[11] a) W. Luo, C. Jiang, Y. Li, S. A. Shevlin, X. Han, K. Qiu, Y. Cheng, Z. Guo, W. Huang, J. Tang, *J. Mater. Chem. A* **2017**, 5, 2021; b) W. D. Chemelewski, H.-C. Lee, J.-F. Lin, A. J. Bard, C. B. Mullins, *J. Am. Chem. Soc.* **2014**, 136, 2843.

[12] a) W. J. Jiang, S. Niu, T. Tang, Q. H. Zhang, X. Z. Liu, Y. Zhang, Y. Y. Chen, J. H. Li, L. Gu, L. J. Wan, J. S. Hu, *Angew. Chem. Int. Ed.* **2017**, 56, 6572; b) L. Zhuang, *Acta Phys.-chim. Sin.* **2017**, 33, 1501; c) C. Dong, T. Kou, H. Gao, Z. Peng, Z. Zhang, *Adv. Energy Mater.* **2017**, 8, 1701347.

Author Manuscript

This article is protected by copyright. All rights reserved.

[13] a) K. Fan, Y. Ji, H. Zou, J. Zhang, B. Zhu, H. Chen, Q. Daniel, Y. Luo, J. Yu, L. Sun, *Angew. Chem. Int. Ed.* **2017**, 56, 3289; b) C. Panda, W. Menezes Prashanth, C. Walter, S. Yao, E. Miehlich Matthias, V. Gutkin, K. Meyer, M. Driess, *Angew. Chem. Int. Ed.* **2017**, 56, 10506.

[14] M. Gong, Y. Li, H. Wang, Y. Liang, J. Z. Wu, J. Zhou, J. Wang, T. Regier, F. Wei, H. Dai, *J. Am. Chem. Soc.* **2013**, 135, 8452.

[15] H. Wang, H. Lee, Y. Deng, Z. Lu, P. Hsu, Y. Liu, D. Lin, Y. Cui, *Nat. Commun.* **2015**, 6, 7261.

[16] Y. Jia, L. Zhang, G. Gao, H. Chen, B. Wang, J. Zhou, T. Soo Mun, M. Hong, X. Yan, G. Qian, J. Zou, A. Du, X. Yao, *Adv. Mater.* **2017**, 29, 1700017.

[17] X. Long, J. Li, S. Xiao, K. Yan, Z. Wang, H. Chen, S. Yang, *Angew. Chem. Int. Ed.* **2014**, 126, 7714.

[18] M. Y. Gao, J. R. Zeng, Q. B. Zhang, C. Yang, X. T. Li, Y. X. Hua, C. Y. Xu, *J. Mater. Chem. A* **2018**, 6, 1551.

[19] J. Wang, L. Gan, W. Zhang, Y. Peng, H. Yu, Q. Yan, X. Xia, X. Wang, *Sci. Adv.* **2018**, 4, 7970.

[20] J. Zhang, T. Wang, P. Liu, Z. Liao, S. Liu, X. Zhuang, M. Chen, E. Zschech, X. Feng, *Nat. Commun.* **2017**, 8, 15437.

[21] C. C. L. McCrory, S. Jung, J. C. Peters, T. F. Jaramillo, *J. Am. Chem. Soc.* **2013**, 135, 16977.

Author Manuscript

This article is protected by copyright. All rights reserved.

Author Manuscript

3D hierarchical NiFe(OH)$_x$/FeS/IF electrode with a nano/micro sheet-on-sheet structure exhibits superior OER activity and durability with a low overpotential of 261 mV at 100 mA cm^{-2} and 332 mV at 1000 mA cm^{-2}. The water-alkali electrolyzer using it as anode achieves stable overall water splitting at 300 mA cm^{-2} with a small cell voltage.

Keyword: hierarchical nano/micro nanostructures, sheet-on-sheet, FeS, oxygen evolution reaction, water splitting

Shuai Niu, Wen-Jie Jiang, Tang Tang, Lu-Pan Yuan, Hao Luo, and Jin-Song Hu*

Autogenous Growth of Hierarchical NiFe(OH)$_x$/FeS Nanosheet-on-Microsheet Arrays for Synergistically Enhanced High-Output Water Oxidation

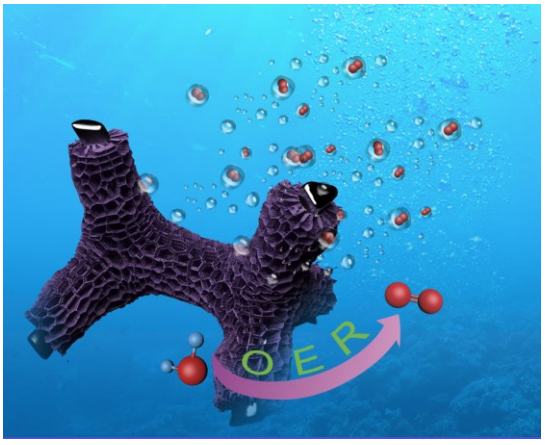

This article is protected by copyright. All rights reserved.